Dalton Transactions

PAPER

View Article Online
View Journal

Cite this: DOI: 10.1039/c5dt04213e

Silver(I), gold(I) and palladium(II) complexes of a NHC-pincer ligand with an aminotriazine core: a comparison with pyridyl analogues†

Jamila Vaughan,[a] Damien J. Carter,*[b] Andrew L. Rohl,[c] Mark I. Ogden,[a] Brian W. Skelton,[d] Peter V. Simpson*[a] and David H. Brown*[a]

Received 27th October 2015,
Accepted 20th November 2015

DOI: 10.1039/c5dt04213e

www.rsc.org/dalton

Dinuclear silver, di- and tetra-nuclear gold, and mononuclear palladium complexes with chelating C,N,C diethylaminotriazinyl-bridged bis(NHC) pincer ligands were prepared and characterised. The silver and gold complexes exist in a twisted, helical conformation in both the solution- and the solid state. In contrast, an analogous dinuclear gold complex with pyridyl-bridged NHCs exists in a linear conformation. Computational studies have been performed to rationalise the formation of twisted/helical *vs.* linear forms.

Introduction

N-Heterocyclic carbene (NHC) metal complexes are prevalent in modern organic and organometallic chemistry.[1,2] With examples that span the majority of the d-block elements, NHC–metal complexes have been investigated for a range of applications and uses, including catalysis (particularly Pd and Ru),[3–8] as precursors to other metal complexes (Ag)[9,10] and more recently biomedical applications (mainly Au and Ag) as antibacterial, anticancer, and antiparasitical agents.[11–15]

The synthesis of NHCs bearing pyridyl donor groups has been of considerable interest, and they have been explored in-depth – either bound directly to the NHC ring (as in **1**), or with a spacer (often methylene).[16] In particular, the imidazole-based NHC-pyridine 'pincer' **1** has been coordinated to a diverse range of metal centres,[17–22] and in many cases the resulting complexes have been used for catalysis applications. These examples have focused on the use of imidazole derived NHCs and it was not until more recently that directly bonded benzimidazolinylidene-pyridyl pincers (*e.g.* **2**) were reported.[23–27]

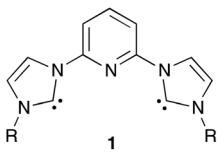

1

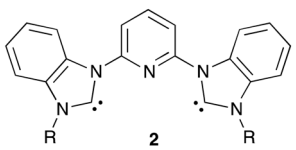

2

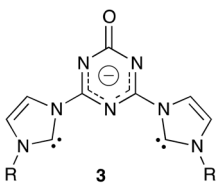

3

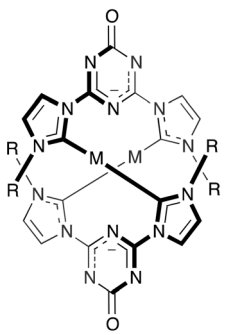

4a (M = Ag)
4b (M = Au)

Recently, the group of Strassner reported dinuclear silver and gold complexes containing bis(NHC) ligands incorporating anionic triazinone bridging units, where the negative charge is delocalised over the triazinone ring (*e.g.* **3** and **4a,b**).[28,29] Short M–N contacts exist between the metal and the closest triazinone nitrogen atom, suggesting a significant interaction that may contribute to the formation of the twisted "double helical" conformation observed in the solid-state. This double

[a]*Department of Chemistry, Curtin University, GPO Box U1987, Perth WA 6845, Australia. E-mail: peter.simpson@curtin.edu.au, d.h.brown@curtin.edu.au, d.carter@curtin.edu.au*
[b]*Science & Maths Education Centre, Nanochemistry Research Institute & Department of Chemistry, Curtin University, GPO Box U1987, Perth WA 6845, Australia*
[c]*Curtin Institute for Computation, Nanochemistry Research Institute & Department of Chemistry, Curtin University, GPO Box U1987, Perth WA 6845, Australia*
[d]*Centre for Microscopy, Characterisation and Analysis, The University of Western Australia, 35 Stirling Highway, Crawley, WA 6009, Australia*

† Electronic supplementary information (ESI) available: Full cif files. Crystal and structure refinement data of all structures and a projection of **5**·2PF$_6$. CCDC 1430963 (**5**·2PF$_6$), 760649 (**6**·2PF$_6$), 1430964 (**7**·2PF$_6$), 1430965 (**8**·2PF$_6$), 1430966 (**9**·PF$_6$) and 1430967 (**11**·2BPh$_4$). For ESI and crystallographic data in CIF or other electronic format see DOI: 10.1039/c5dt04213e

helical, or twisted, conformation is also commonly observed for pyridyl-bridged bis(NHC) dinuclear complexes,[22,25,30,31] and is thought to form *via* the reaction of the mono-carbene intermediate with another equivalent of the intermediate. Here we complement Strassner's initial study by reporting the preparation of several silver, gold, and palladium complexes bearing bis(NHC) diethylaminotriazinyl-bridged pincer ligands, as well as a gold complex bearing a bis(NHC) pyridyl-bridged pincer ligand. We also describe a detailed computational, and solution- and solid-state, investigation of the propensity of these types of complexes to form "double helical" twisted, or non-twisted linear conformations.

Results and discussion

Synthesis

The reaction of 1-butylbenzimidazole with 1,3-dichloro-5-diethylaminotriazine in acetonitrile afforded the benzimidazolium salt **5**·2Cl in high yield (92%), which was converted to **5**·2PF_6 by salt metathesis with potassium hexafluorophosphate in water. In the crystal structure of **5**·2PF_6 (Fig. S1†) the two imidazolium units are hydrogen bonded through each H2 atom to a fluorine atom of the hexafluorophosphate anion, which could give an indication that coordination to a metal at this position is favoured upon deprotonation.[32] The reaction of **5**·2PF_6 with silver oxide in acetonitrile, in the presence of 3 Å molecular sieves, afforded the dinuclear silver(I) complex salt **6**·2PF_6 in 64% yield (Scheme 1). The salt was isolated as a white powder and could be recrystallised to afford colourless crystals. The salt readily dissolves in polar solvents such as acetone and acetonitrile.

Reaction of the silver(I) complex salt **6**·2PF_6 with bromido(tetrahydrothiophene)gold(I) in acetonitrile afforded the gold(I) complex salt **7**·2PF_6 as yellow powder (Scheme 2). Recrystallisation of the yellow powder afforded a mixture of two different types of crystals. The bulk of the crystals were colourless and confirmed by NMR and single-crystal X-ray studies (see below) to be the **7**·2PF_6. A very minor component of the crystals were bright yellow, which were confirmed by single X-ray studies to be a tetranuclear gold complex **8**·2PF_6 (Scheme 3, Solid-state studies section). The crystal structure of **8**·2PF_6 was modelled

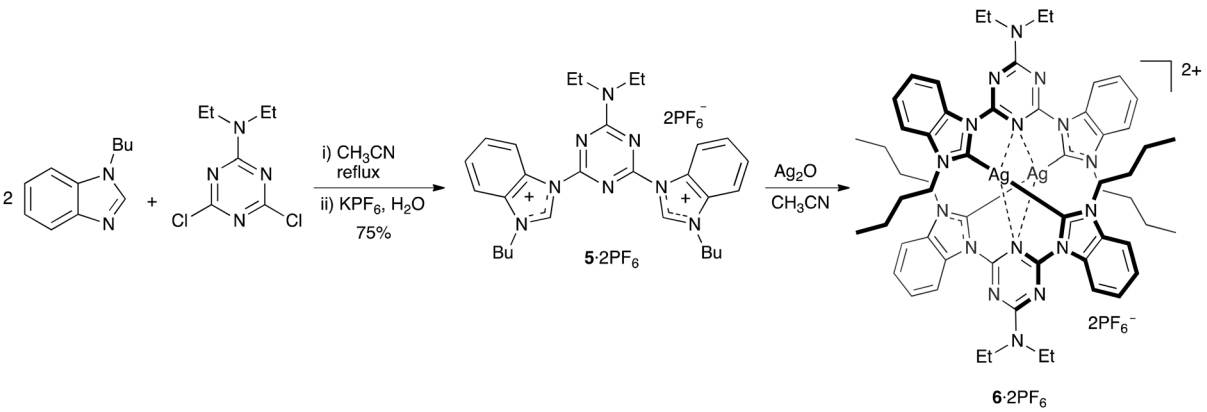

Scheme 1 Synthesis of dinuclear silver complex **6**·2PF_6.

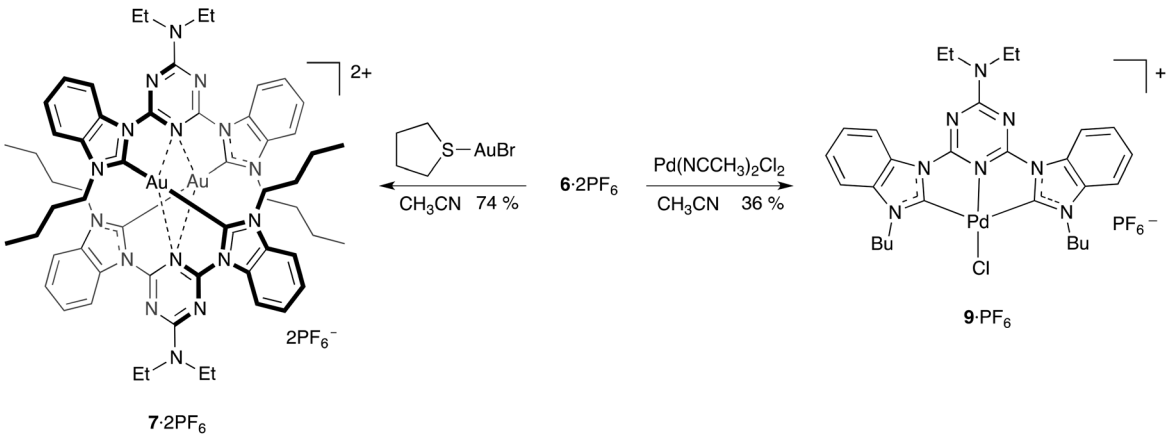

Scheme 2 Synthesis of silver and palladium complexes **7**·2PF_6 and **9**·PF_6.

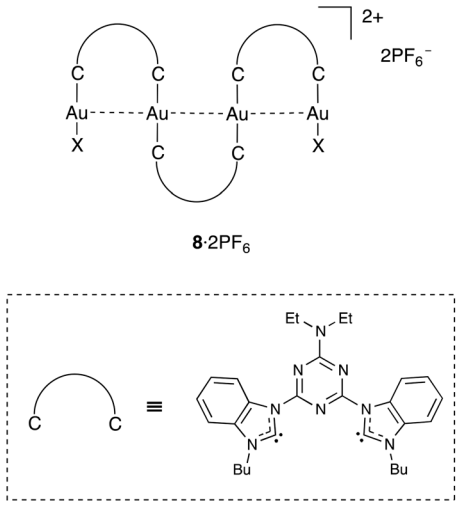

Scheme 3 Tetranuclear gold complex **8** (X = Br/Cl).

as a 50 : 50 mixed Br/Cl, with the chloride impurity possibly arising from incomplete salt metathesis of **5**·2Cl or during the preparation of bromido(tetrahydrothiophene)gold(I). Numerous attempts to prepare **8** by variations of procedures and reagent ratios lead only to the formation of **7**·2PF_6 with only trace quantities of **8**·2PF_6. The tetranuclear complex salt **8**·2PF_6 could only be isolated by manual separation of the yellow crystals that formed as a minor component during the purification of the bulk material **7**·2PF_6. The silver complex **6**·2PF_6 could also undergo transmetallation with palladium(II) chloride in acetonitrile to afford the mono-nuclear palladium complex **9**·PF_6 (Scheme 2).

We have previously reported the silver(I) complex **10**·2BPh_4.[25] To enable comparison of the triazinyl-pincer complexes with their pyridyl analogues we also prepared the dinuclear gold(I) complex **11**·2BPh_4 by reaction of **10**·2BPh_4 with bromido(tetrahydrothiophene)gold(I) in acetonitrile, which was isolated as colourless powder/crystals (Scheme 4). The complex adopt a linear type structure (see Solid state studies section), similar to other dinuclear gold(I) complexes of bis (NHC) ligands bridged by *para*-phenyl, stilbenyl, and anthracenyl groups.[33–35]

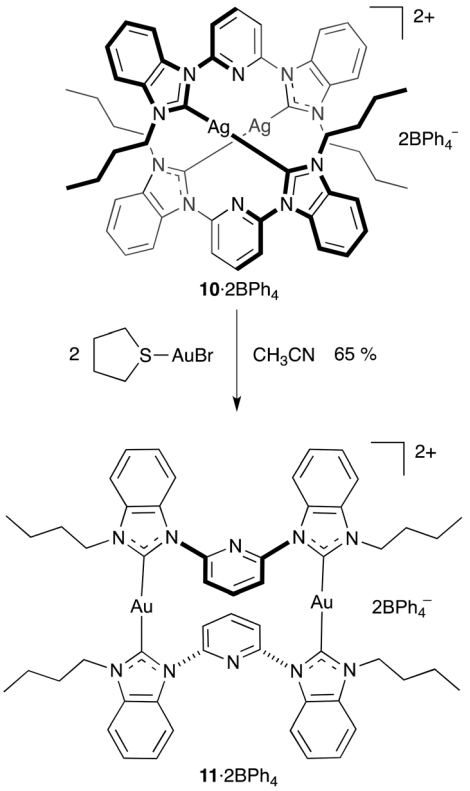

Scheme 4 Synthesis of **11**·2BPh_4.

NMR studies

The ^{1}H NMR spectrum of a solution of **6**·2PF_6 in CD_3CN displays signals consistent with the structure, however, of particular interest is the signal for the methyl groups of the butyl chain, which has an up-field chemical shift of δ 0.34 (δ 0.26 in d_6-DMSO). This up-field shift, when compared to the analogous signal for **5**·2PF_6 (δ 0.98 in d_6-DMSO), is attributed to magnetic shielding of the butyl chain by the aromatic groups on the opposing ligand in the dinuclear structure. The proximity of the butyl chain and the aromatic groups is observed in the solid-state structure. These observations indicate that the 'twisted' dinuclear structure of **6** is prevalent in solution, and not just the solid-state. Similar observations were made with the pyridine analogue **10**.[25] The ^{13}C NMR spectrum of a solution of **6**·2PF_6 in CD_3CN (or d_6-DMSO) displayed two sharp doublets, centred at δ 194, for the carbene carbons (J = 187 and 215 Hz), consistent with coupling to ^{107}Ag and ^{109}Ag.[10] In addition to the splitting of the carbene carbon signal, for solutions in d_6-DMSO, the signals for the bridge-head carbons of the benzimidazole ring (C8 and C9) appear as doublets (splitting 4 and 6 Hz), consistent with three-bond coupling to the silver. The sharp carbene carbon signals and the long range coupling suggest that the Ag–carbene bonds are relatively strong, or that the silver-centres are held in the complex in a static environment. Previous studies have suggested that the lack of C–Ag coupling may be due to labile Ag–C bonds.[36,37] It may be possible that weak N···Ag interactions involving the triazine in **6** (see below) help to stabilise the complex. Two similar 'twisted' dinuclear structures, **10**[25] and [$\mathbf{1}_2Ag_2$]$^{2+}$,[31,38] do not display the long-range coupling, and in both cases the contacts between the pyridyl nitrogens and the silver centres are longer than those in **6**.

The ^{1}H NMR spectrum of a solution of the gold–triazinyl–NHC pincer complex **7**·2PF_6 in CD_3CN displays signals similar to that of the silver analogue **6**·2PF_6. The signals of the methyl groups are up-field at δ 0.34, suggesting that the gold complex also exists in the twisted conformation in solution, as well as in the solid-state (see Solid-state studies section). As would be expected for gold(I) complexes, the signal for the carbene carbons is a singlet at δ 192. Interestingly the ^{1}H NMR spec-

trum of a solution of the gold–pyridyl–NHC pincer complex **11**·2BPh$_4$ in d_6-DMSO displays a signal attributed to the methyl groups of the butyl chain at δ 0.82, downfield in comparison to the analogous signal in the triazinyl complex **7**·2PF$_6$. The more conventional chemical shift for an alkyl methyl group in **11** is consistent with the absence of magnetic shielding and suggests that in solution the dinuclear gold–NHC–pyridyl pincer complex **11** adopts a non-twisted conformation, presumably similar to that identified in the solid-state for **11** (see Solid-state studies section). As expected the ^{1}H NMR spectrum of a solution of the mononuclear palladium complex **9**·PF$_6$ in d_6-DMSO displays a signal attributed to the methyl groups of the butyl chain at δ 0.87. In this case no magnetic shielding of the methyl group is possible.

Luminescence studies

The luminescence of the gold(I) complexes was studied, and is shown in Fig. 1. It proved extremely difficult to completely separate the two triazinyl–NHC pincer gold(I) complexes **7**·2PF$_6$ and **8**·2PF$_6$, with manual separation of a crystalline mixture proving the only adequate method. Still, quantitative photophysical measurements could not be made due to small amounts of contamination present in the crystals. Solid-state luminescence studies indicated that the tetra-nuclear complex **8**·2PF$_6$ was highly emissive (λ_{em} = 528 nm) whereas the dinuclear complexes **7**·2PF$_6$ and **11**·2BPh$_4$ did not exhibit any significant luminescence. The shorter Au···Au contact in **8** is presumably responsible for the luminescence (see Solid-state studies).

Solid-state studies

The cation **6** is shown in Fig. 2 (with selected geometries) and consists of a $[Ag_2L_2]^{2+}$ dimer with the benzimidazolin-2-ylidene groups of each ligand coordinated to different Ag atoms. There is also one molecule of acetonitrile per dimer in the lattice. The structure is similar to that of the pyridine analogue **10**, except that the N(n21) atoms of the triazine groups are now weakly coordinated to the Ag atoms [Ag(1)–N(121), N(221) 2.786(3), 2.899(2) Å and Ag(2)–N(121), N(221) 2.880(2), 2.764(2) Å; *cf.* **10**:[25] Ag···N 2.984(1), 3.012(1)]. As a result of these interactions, the C–Ag–C angles now deviate significantly from linearity, the C(112)–Ag(1)–C(232) and C(132)–Ag(2)–C(212) angles being 165.51(11) and 164.74(13)° respectively. The Ag(1)···Ag(2) distance has also been substantially reduced to 3.0899(3) Å *cf.* 3.7848(2) Å for **10**. The orientations of the pendant rings in **6** are twisted relative to the central plane, but less than those of **10**. The angles between the planes of the pendant groups and the central triazine rings are 14.19(9) and 31.32(9)° (ligand 1) and 18.64(8) and 26.29(8)° (ligand 2) compared with 42.57(4) and 39.91(4)° in **10**.

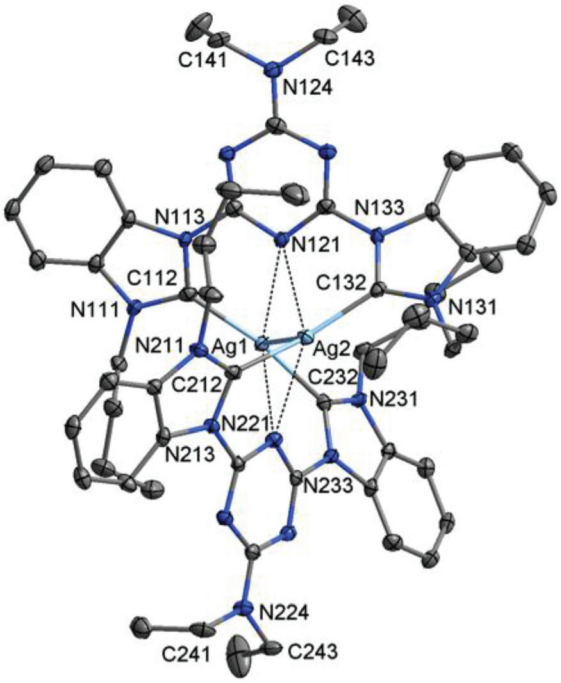

Fig. 2 Projection of the cation **6**. Ellipsoids displayed at 50% probability; hydrogen atoms have been omitted for clarity. Selected bond distances (Å) and angles (°): Ag(1)–C(112) 2.098(3), Ag(1)–C(232) 2.100(3), Ag(1)···N(121) 2.786(3), Ag(1)···N(221) 2.899(2), Ag(1)···Ag(2) 3.0899(3), Ag(2)–C(132) 2.085(2), Ag(2)–C(212) 2.097(3), Ag(2)···N(121) 2.880(2), Ag(2)···N(221) 2.764(2), C(112)–Ag(1)–C(232) 165.51(11), C(132)–Ag(2)–C(212) 164.74(13).

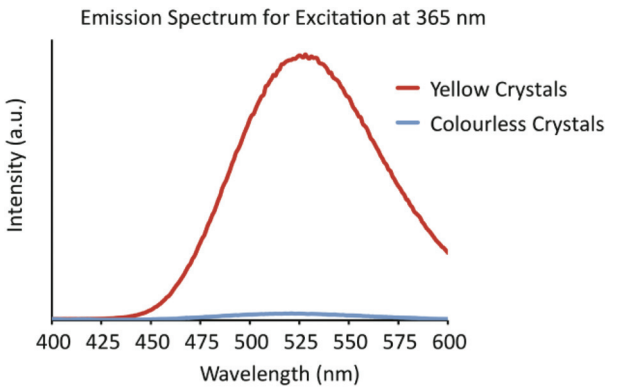

Fig. 1 Emission of **8**·2PF$_6$ (red trace) and **7**·2PF$_6$ upon excitation at 365 nm.

The bond lengths of the diethylaminotriazine moiety (see Fig. 3), and the co-planar arrangement of the N(CH$_2$)$_2$ units with respect to the triazine rings, suggest the influence of a pyridone–iminium resonance structure.[39] A contribution of this structure would result in the enhancement of the nucleophilicity of the ring-nitrogen *para* to the diethylamino groups. Such enhanced nucleophilicity may explain the shorter N···Ag contacts observed in **6**, compared to that of **10**.

The structure of silver complex **6** begs comparison with those of triazinone- and pyridyl-bridged bis(NHC)–Ag complexes **4a**[28] and **10**,[25] respectively (Fig. 4). Although the NHC ligands in **4a** contain different *N*-substituents and are derived from imidazole rather than benzimidazole for **6** and **10**, the electronic effects caused by the three types of bridging

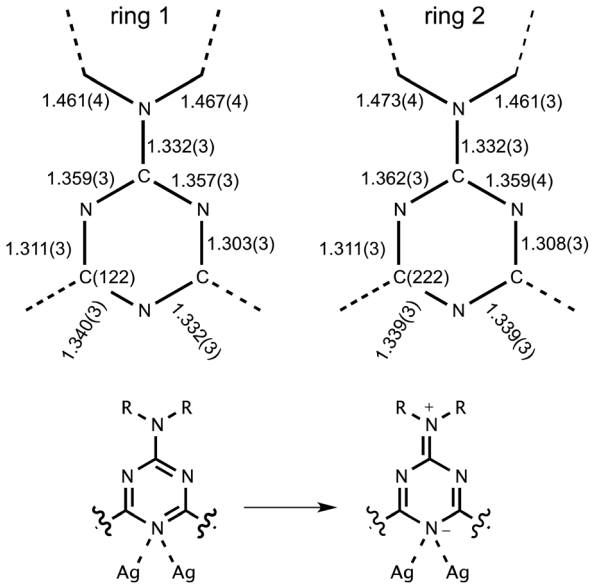

Fig. 3 Bond lengths for the aminotriazine moieties of **6**, and a possible resonance contribution to the structure.

heterocycles contribute significantly to the overall geometry around the Ag–Ag core. The enhanced nucleophilicity of the triazinyl nitrogen in **6**, due to the pyridine–iminium resonance form, leads to short N–Ag contacts, and also contribute to a shortening of the Ag–Ag bond. Similarly, in **4a**, the formal negative charge on the triazinyl nitrogen presumably leads to short N–Ag contacts and a short Ag–Ag bond. Therefore, the core geometries around **6** and **4a** are very similar, with only a slight shortening of the Ag–Ag bond in **4a** relative to **6**. The relatively weak nucleophilicity of the pyridyl nitrogen in **10** *cf.* **6** and **4a** leads to longer N–Ag contacts and a greater Ag–Ag distance. For completeness, it is worth noting that although Ag–N interactions are present in these pincer compounds, in other cases involving close d^{10} metal–arene contacts, proximity alone does not always indicate the presence of agnostic interactions.[40]

The cation of **7** is shown in Fig. 5 and consists of a $[Au_2L_2]^{2+}$ dimer with the benzimidazolin-2-ylidene groups of each ligand coordinated to different Au atoms. There is also one molecule of acetonitrile per dimer in the lattice. The structure is isomorphous with that of the silver analogue **6**. The triazine groups are weakly coordinated to the Au atoms, Au(1)–N(121), N(221) 2.902(4), 2.945(3) Å and Au(2)–N(121), N(221) 2.937(3), 2.890(3) Å, while the Au(1)···Au(2) distance is 3.3955(4) Å. In the same way that the aminotriazinyl- and triazinone-bridged silver complexes displayed similar core geometries, the analogous distances in **7** are similar to those for gold triazinone complex **4b**, also reported by Strassner and co-workers.[29] As a result of these interactions, the C–Au–C angles now deviate significantly from linearity, the C(112)–Au(1)–C(232) and C(132)–Au(2)–C(212) angles being 170.50(15) and 170.58(17)°, respectively, but with less deviation than the corresponding values in the Ag analogue **6**. The orientations of the pendant rings are twisted relative to the central plane. The angles between the planes of the pendant groups and the central triazine rings are 16.0(1) and 32.9(1)° (ligand 1) and 20.3(1) and 27.5(1)° (ligand 2) and similar to those of **6**.

The cation **11**, where pyridyl groups now bridge the NHC units, adopts a very different conformation to that of **7**, and is seen in Fig. 6. The cation consists of a $[Au_2L_2]^{2+}$ dimer situated on a crystallographic inversion centre with the benzimidazo-

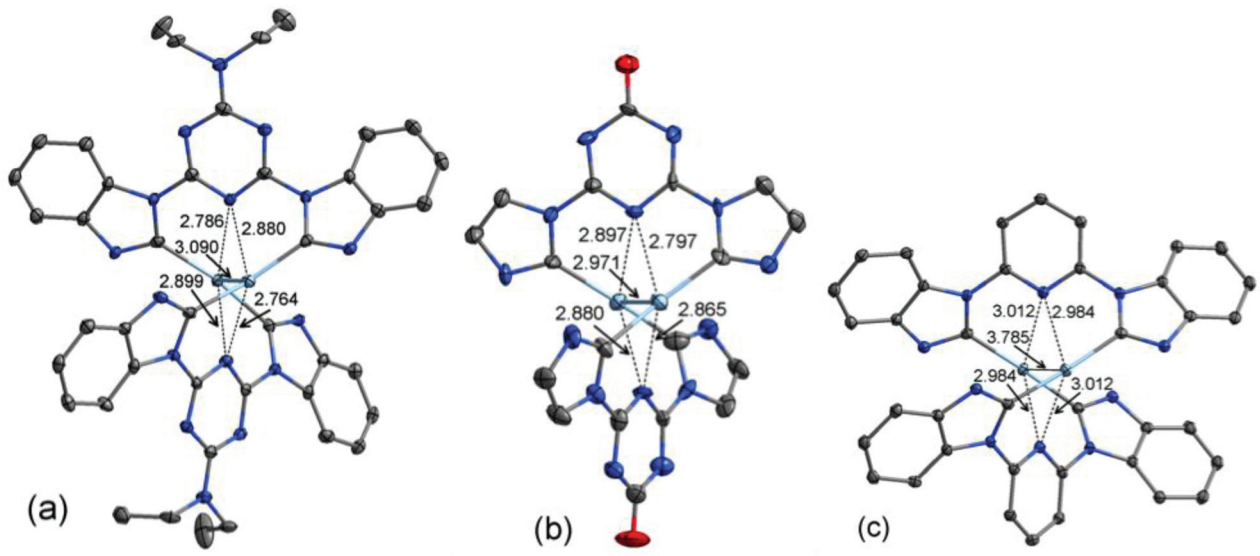

Fig. 4 Projections and selected bond distances (Å) of (a) aminotriazinyl-bridged cation **6**; (b) triazinone-bridge complex **4a** from Strassner and co-workers;[28] and (c) pyridyl-bridged cation **10** from Brown and co-workers.[25] Ellipsoids displayed at the 50% probability level; hydrogen atoms and the (benz)imidazolyl *N*-substituents have been omitted for clarity.

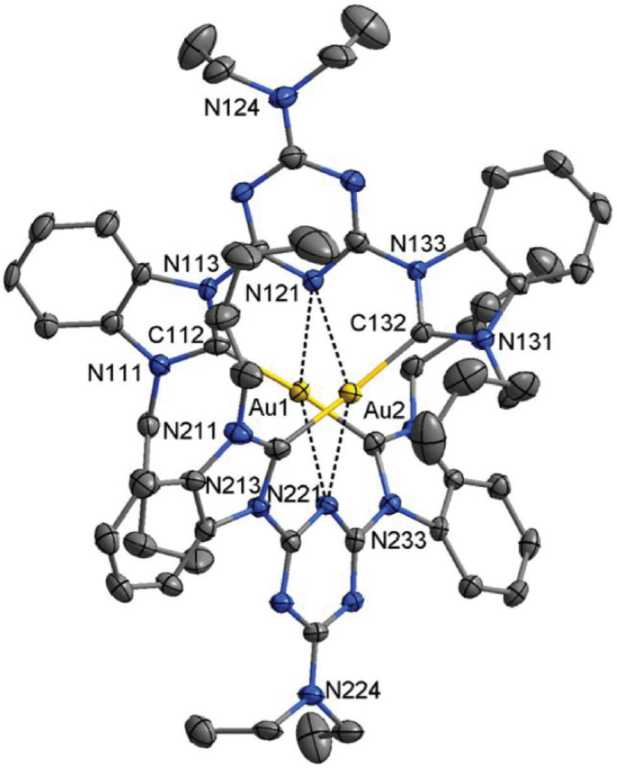

Fig. 5 Projection of the cation **7**. Ellipsoids are displayed at the 50% probability level; hydrogen atoms have been omitted for clarity. Selected bond distances (Å) and angles (°): Au(1)–C(112) 2.023(4), Au(1)–C(232) 2.025(4), Au(1)···N(121) 2.902(4), Au(1)···N(221) 2.945(3), Au(1)···Au(2) 3.3955(5), Au(2)–C(132) 2.009(3), Au(2)–C(212) 2.027(3), Au(2)···N(121) 2.937(3), Au(2)···N(221) 2.890(4), C(112)–Au(1)–C(232) 170.50(15), C(132)–Au(2)–C(212) 170.58(17).

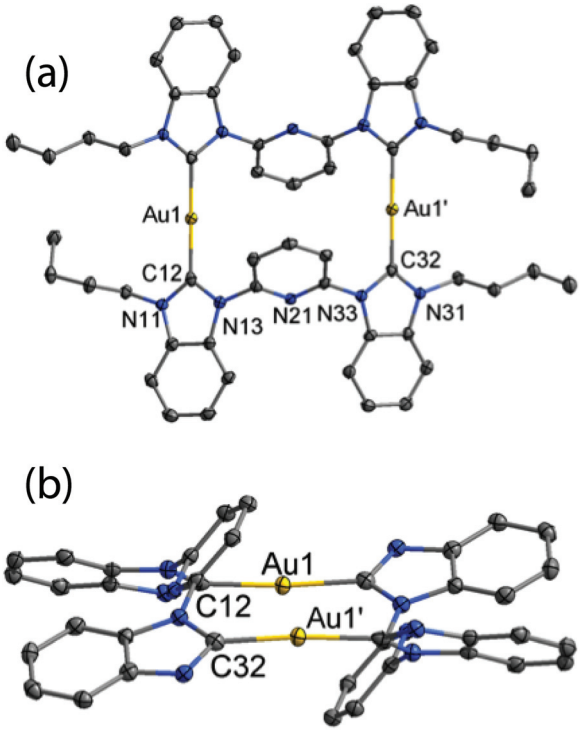

Fig. 6 Projections of the cation **11** showing (a) the top view of the molecule and (b) the side view, highlighting the 'V' shaped nature of the benzimidazolyl units. Ellipsoids are displayed at the 50% probability level; hydrogen atoms and the butyl chains in (b) have been omitted for clarity. Selected bond distances (Å) and angles (°): Au(1)–C(12) 2.006(2), Au(1)–C(32′) 2.012(3), C(12)–Au(1)–C(32′) 175.43(9).

lin-2-ylidene groups of each ligand coordinated to different Au atoms. Thus, the coordination about the Au atom is essentially linear, with the C12–Au1–C32′ angle being 175.43(9)°, the prime referring to the centrosymmetrically related atom at $1-x, 1-y, 1-z$. Relevant geometries are given in the caption of Fig. 6. Since the molecule is situated on an inversion centre, the four coordinated carbon atoms are coplanar, the Au(1) deviation from this plane being 0.080(2) Å. The ligand is not planar, but forms a 'V' shape (see Fig. 6(a and b)), with the pyridyl ring at the base. The angles between the coordination Au_2C_4 plane and the planes of the two pendant rings are 27.93(5)° and 28.53(5)°. The Au(1)–N(22) distances are greater than 4 Å, indicative of no interaction, while the Au1···Au1′ distance of 6.6193(5) Å is too great to lead to any aurophilic interactions. A similar linear conformation of gold atoms albeit with a different pyridyl arrangement has recently been reported for an analogous gold complex with hexyl groups instead of butyl groups on the benzimidazolyl units,[41] and so the helical/twisted nature of observed in **7** may be attributable to the aminotriazinyl bridge. Furthermore, it is interesting to note that similar dinuclear gold complexes where the NHCs are derived from imidazole instead of benzimidazole display a twisted conformation similar to that of **6** and **7**.[22,41]

In the structure of tetranuclear complex **8**, shown in Fig. 7(a), each ligand bridges between two gold atoms with the terminal gold atoms capped by halide ions, thus forming an extended helical structure. Each of the gold atoms is two coordinate with Au–C distances of 1.965(10) and 1.976(9) Å for the terminal gold atoms with those to the central gold atoms lying in the range 2.017(10)–2.033(9) Å. There are, however, weak bridging interactions between the nitrogen atom of each of the triazine groups and adjacent gold atoms; the Au–N distances lie in the range 2.846(7)–2.976(7) Å. The coordination about the gold atoms deviates significantly from linearity with the C–Au–C angles being 175.8(4) and 176.1(4)° and the C–Au–X angles 170.9(3) and 175.5(3)°. The four gold atoms are not linearly arranged with the Au···Au···Au angles being 143.70(2) and 147.07(2)°. The Au···Au distances are Au(1)···Au(2) 3.2101(10), Au(2)···Au(3) 3.2709(7) and Au(3)···Au(4) 3.1395(8) Å. A more in depth discussion of the structure of **8** can be found in the ESI.†

The coordination around the palladium centre in complex **9**, seen in Fig. 8(a), is distorted square planar. The three rings are essentially coplanar with the atoms with the maximum deviations being C(36) (−0.083(1) Å) and C(37) (−0.071(1) Å) with the Pd deviation being 0.017(1) Å. The dihedral angles between the coordination plane and the three rings 1–3 are 1.55(2), 2.26(3) and 3.05(3)°. There is a weak interaction between the PF_6^- anion and the Pd atom, the distance Pd(1)–F(1)

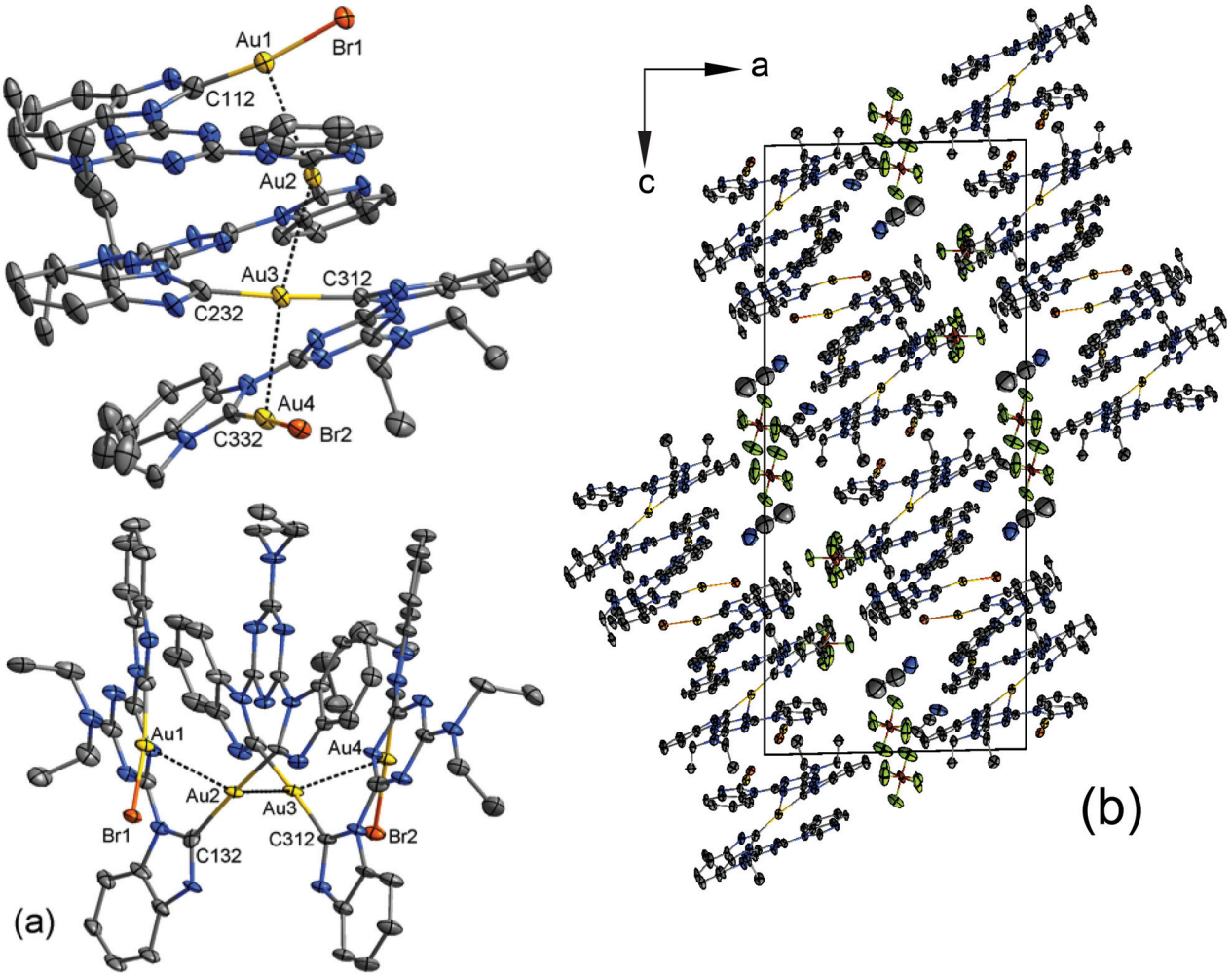

Fig. 7 Projections of (a) cation **8** and (b) crystal packing showing the cations lying in sheets. Ellipsoids are displayed at the 30% probability level; hydrogen atoms and the butyl chains have been omitted for clarity. Selected bond distances (Å) and angles (°): Au(1)–C(112) 1.965(10), Au(1)–Br, Cl(1) 2.3686(14), Au(1)···Au(2) 3.2101(10), Au(2)–C(132) 2.033(9), Au(2)–C(212) 2.033(8), Au(2)···Au(3) 3.2709(7), Au(3)–C(232) 2.017(10), Au(3)–C(312) 2.022(8), Au(3)···Au(4) 3.1395(8), Au(4)–C(332) 1.976(9), Au(4)–Br, Cl(2) 2.3838(13), C(112)–Au(1)–Br, Cl(1) 170.9(3), C(132)–Au(2)–C(212) 175.8(4), Au(1)···Au(2)···Au(3) 143.70(2), C(232)–Au(3)–C(312) 176.1(4), Au(4)···Au(3)···Au(2) 147.07(2), C(332)–Au(4)–Br, Cl(2) 175.5(3).

is 3.2928(7) Å. In the unit cell, there are close approaches of atoms of pairs of centrosymmetrically related cations resembling π-stacking, with the shortest distances being Pd(1)···N (21) 3.4456(9), N(13)···C(32) 3.383(1), N(31)···C(13A) 3.391(1) Å (Fig. 8(b)).

Computational studies

In an effort to find the origin of the intriguing difference in conformation of the silver- and gold–pyridyl–NHC pincer complexes (**10** and **11** respectively), computational studies were carried out. The use of traditional density functional theory (DFT) methods to study soft matter or molecular crystals has in the past been hampered by the lack of potentially important van der Waals (vdW) or dispersion forces. In recent years, the development and improvement of methods to include dispersion forces in DFT now makes this routinely possible. van der Waals corrected DFT calculations of molecular crystals have been used to study a range of solid state systems such as monosaccharides,[42] amino acids,[43] epoxydihydroarsanthrene analogues,[44] polycyclic aromatic hydrocarbons,[45] and many others.[46–53]

There have been a number of gas–phase studies of large supramolecular systems[54–59] using vdW-corrected DFT, with a number of these studies using the S12L set of large dispersion-bound host–guest systems.[58] There are a limited number of studies of large crystalline supramolecular systems, such as calculations of *p-tert*-butylcalix[4]arene inclusion compounds,[60,61] metal organic framework materials[62,63] and rotaxane structures.[64]

In Table 1 we report the lattice parameters of DFT optimised crystal structures of **10**·2BPh_4 and **11**·2BPh_4 containing either Ag or Au metal atoms. The calculated structures compare closely to the corresponding observed experimental crystal structures, with a variation of 0.8–1.5% in the lattice

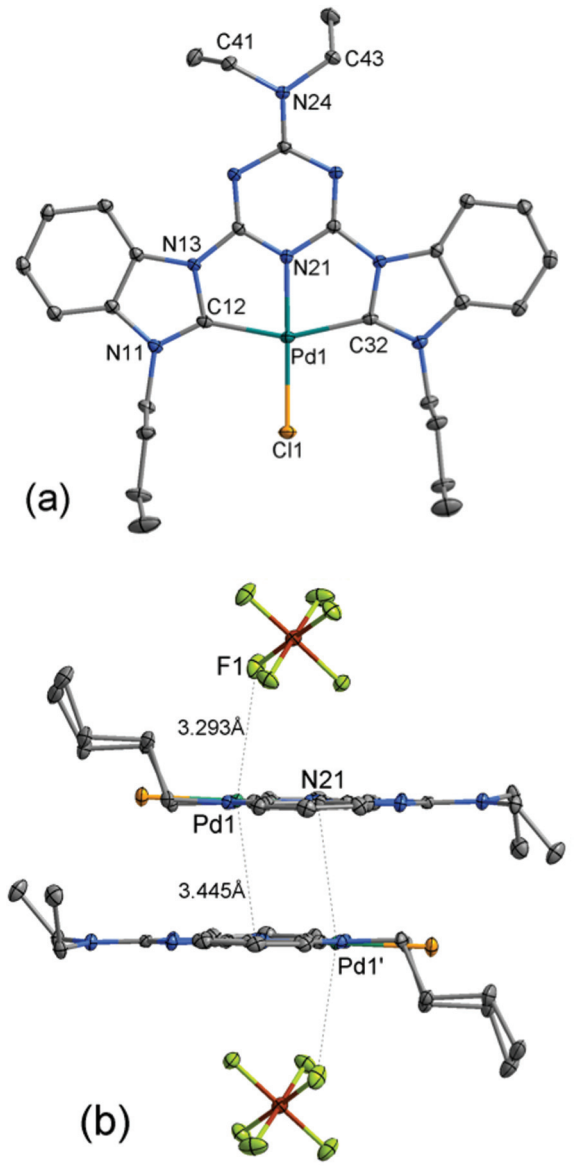

Fig. 8 Projection of (a) the cation **9** and (b) close contacts between centrosymmetrically related molecules of **9**. Ellipsoids are displayed at the 50% probability level; hydrogen atoms have been omitted for clarity. Selected bond distances (Å) and angles (°): Pd(1)–N(21) 1.9497(8), Pd(1)–C(12) 2.0317(10), Pd(1)–C(32) 2.0384(10), Pd(1)–Cl(1) 2.2935(3), N(21)–Pd(1)–C(12) 78.60(3), N(21)–Pd(1)–C(32) 78.01(3), C(12)–Pd(1)–C(32) 156.59(4), N(21)–Pd(1)–Cl(1) 178.61(3), C(12)–Pd(1)–Cl(1) 100.67(3), C(32)–Pd(1)–Cl(1) 102.74(3).

parameters. We have previously reported the excellent performance of the vdW-DF2(rPW86) functional for the C21 reference set of molecular crystals and monosaccharide structures,[42] with mean deviations of the lattice parameters of ~1.2%.

In Table 2 we report the relative interaction energies, corrected for basis set superposition error, for Ag and Au in the isolated **10**·2BPh$_4$ and **11**·2BPh$_4$ ligand structures and the crystal structures. For the isolated complexes, calculations predict the twisted **10** structure is preferred for both Ag and Au

Table 1 DFT optimised lattice parameters of **10**·2BPh$_4$ and **11**·2BPh$_4$ with both Ag and Au as the coordinated atom, compared to the respective experimental crystal structures

	Metal atom	a (Å)	b (Å)	c (Å)	β (°)
10·2BPh$_4$ structure					
Experiment	Ag	24.003	17.332	20.468	104.16
DFT	Ag	24.323 (+1.33%)	17.562 (+1.33%)	20.630 (+0.79%)	104.57 (+0.39%)
DFT	Au	24.357	17.540	20.624	104.31
11·2BPh$_4$ structure					
Experiment	Au	13.415	17.869	17.508	100.72
DFT	Au	13.610 (+1.45%)	18.106 (+1.32%)	17.731 (+1.27%)	100.46 (−0.26%)
DFT	Ag	13.690	18.012	17.700	100.06

Table 2 Relative interaction energies of Ag and Au in isolated complexes and the crystal structures of **10**·2BPh$_4$ and **11**·2BPh$_4$

		Relative interaction energy (kJ mol^{-1}) per metal atom	
Metal atom	Ligand structure	Isolated	Crystal
Ag	**10**·2BPh$_4$ (twisted)	0.00	0.00
	11·2BPh$_4$ (non-twisted)	+20.27	+1.00
Au	**10**·2BPh$_4$ (twisted)	0.00	+12.21
	11·2BPh$_4$ (non-twisted)	+13.31	0.00

atoms by 20.27 and 13.31 kJ mol^{-1} (per metal atom), respectively. In the crystal structure, the relative interaction energies show that Ag is more stable in the twisted **10**·2BPh$_4$ structure by 1.00 kJ mol^{-1} (per metal atom), and Au is more stable in the non-twisted **11**·2BPh$_4$ structure by 12.21 kJ mol^{-1} (per metal atom). This trend in relative interaction energies matches exactly with the experimental observations of the stable crystal structures, and solution phase studies, observed for Ag and Au atoms with the two different ligand environments. The 1 kJ mol^{-1} preference of Ag metal for the twisted **10**·2BPh$_4$ structure is significant, as although we found an average lattice energy error of 3.85 kJ mol^{-1} for the C21 reference set of molecule crystals,[42] for systems containing the same species in the same amounts, the relative error will be much smaller due to error cancellation.

Examining in more detail the isolated ligand structures, it is perhaps not unsurprising to see that the twisted **10** structure is preferred for both Ag and Au. In the isolated case, the ligand backbone is free to contort to accommodate the coordinated metal atoms, without any interaction with the crystal environment or solvation considerations. The metal atom–metal atom distances in the isolated complexes are noticeably shorter than those found in the corresponding calculated crystal structure, with the Ag–Ag separation distance shortening from 4.14 to 3.16 Å and the Au–Au separation

distance shortening from 4.23 to 3.54 Å. The shorter metal atom–metal atom distances indicate a stronger "metallophillic" interaction between the metal atoms in the isolated structures. These metallophillic interactions between two d^{10} metal centres have been recently reviewed.[65,66] In the less-favoured, isolated, non-twisted **11** structure, the metal atom–metal atom distances increased slightly compared to those in the corresponding calculated crystal structure, with the Ag–Ag separation distance increasing from 6.78 to 7.16 Å and the Au–Au separation distance increasing from 6.83 to 7.15 Å. The metal atom–N atom distances and metal atom–C atom distances in both the isolated complexes and crystal structures are largely unaffected by the choice of Ag or Au coordinating atoms, with only very minor variations in separation distances. Based on these calculations, the crystal environment (or solvation in solution) plays a significant but subtle role in determining the conformation of these metal complexes.

Conclusion

We have reported the synthesis of several silver, gold, and palladium bis(NHC) complexes containing a pyridyl- or diethylaminotriazinyl-bridge. The introduction of the triazine moiety has resulted in significant structural changes compared to a pyridine analogue. Solution- and solid-state studies have revealed that the triazinyl containing gold complexes adopt a twisted, "helical" conformation, while simple pyridyl-bridged systems are linear. Computational studies suggest that the twisted conformation is generally more stable *in vacuo*, and the crystal environment stabilises the linear conformation in the gold pyridyl-bridged systems; an exception being in gold complexes containing imidazole-based carbene ligands, which also crystallise in the twisted form. In contrast, the analogous silver complex is more stable in the helical conformation in isolation, and in the crystal environment. The remarkable tetranuclear gold complex **8** was also synthesised in trace amounts as a by-product in the preparation of **7**, and was characterised by X-ray studies.

Experimental

General methods

Nuclear magnetic resonance spectra were recorded using Varian Gemini 200 (200 MHz for ^{1}H, 50 MHz for ^{13}C), Bruker AVN 400 (400.1 MHz for ^{1}H, 100.6 MHz for ^{13}C), Bruker Avance 500 (500.1 MHz for ^{1}H, 125.8 MHz for ^{13}C) or Bruker Avance 600 (600.1 MHz for ^{1}H, 150.9 MHz for ^{13}C) spectrometers at ambient temperature. ^{1}H and ^{13}C chemical shifts were referenced to residual solvent resonances. Microanalyses were performed by the Central Science Laboratory at the University of Tasmania or by Mr Robert Herman at the Department of Chemistry, Curtin University. UV-vis data was collected on a PerkinElmer LAMBDA 35 UV/VIS spectrometer. 1-*n*-Butylbenzimidazole,[67] 1,3-dichloro-5-diethylaminotriazine,[68] bromido(tetrahydrothiophene)gold(I)[69] and the silver complex **10**·2BPh$_4$ [25] were prepared by literature procedures.

Synthesis of 1,1′-[2,6-(4-diethylaminotriazinyl)]di(3-*n*-butylbenzimidazolium) dichloride 5·2Cl. A solution of 1-*n*-butylbenzimidazole (1.25 g, 7.2 mmol) in acetonitrile (5 mL) was added to a solution of 1,3-dichloro-5-diethylaminotriazine (0.58 g, 2.6 mmol) in acetonitrile (5 mL). The resulting solution was heated at reflux overnight. The solution was then cooled and diluted with diethyl ether (20 mL). The resulting precipitate was collected, washed with diethyl ether (3 × 15 mL) and dried under vacuum to afford a white powder (1.45 g, 92%). δ_H (200 MHz; d_6-DMSO) 0.96 (6 H, t, *J* 8, 2 × $CH_2CH_2CH_3$), 1.40 (6 H, t, *J* 6, 2 × NCH_2CH_3), 1.44 (4 H, m, 2 × $CH_2CH_2CH_3$), 2.05 (4 H, m, 2 × NCH_2CH_2), 3.96 (4 H, q, *J* 6, 2 × NCH_2CH_3), 4.81 (4 H, t, *J* 8, 2 × NCH_2CH_2), 7.80–7.96 (4 H, m, 4 × Ar CH), 8.31 (2 H, d, *J* 8, 2 × Ar CH), 8.72 (2 H, d, *J* 8, 2 × Ar CH) and 12.32 (2 H, s, NCHN); δ_C (50 MHz; d_6-DMSO) 12.3 (CH_3), 13.3 (CH_3), 19.0 (CH_2), 30.5 (CH_2), 43.4 (CH_2), 47.5 (CH_2), 114.6 (CH), 117.0 (CH), 127.5 (CH), 128.7 (CH), 128.8 (C), 132.2 (C), 144.7 (CH), 160.7 (C) and 164.0 (C); (Found: C, 57.41; H, 7.00; N, 18.58. $C_{29}H_{38}N_8Cl_2·2H_2O$ requires C, 57.52; H, 6.99; N, 18.50%).

Synthesis of 1,1′-[2,6-(4-diethylaminotriazinyl)]di(3-*n*-butylbenzimidazolium) bis(hexafluoro-phosphate) 5·2PF$_6$. A solution of **5**·2Cl (0.23 g, 0.40 mmol) in water (10 mL) was added to a solution of KPF_6 (0.45 g, 2.4 mmol) in water (10 mL). The resulting precipitate was collected, washed with water (2 × 10 mL) and diethyl ether (3 × 10 mL), and dried to afford a white powder (0.26 g, 82%). δ_H (200 MHz; d_6-DMSO) 0.98 (6 H, t, *J* 7, 2 × $CH_2CH_2CH_3$), 1.38 (6 H, t, *J* 7, 2 × NCH_2CH_3), 1.49 (4 H, m, 2 × $CH_2CH_2CH_3$), 2.02 (4 H, m, 2 × NCH_2CH_2), 3.97 (4 H, q, *J* 7, 2 × NCH_2CH_3), 4.73 (4 H, t, *J* 8, 2 × NCH_2CH_2), 7.82–7.97 (4 H, m, 4 × Ar CH), 8.33 (2 H, d, *J* 7, 2 × Ar CH), 8.76 (2 H, d, *J* 7, 2 × Ar CH) and 10.77 (2 H, s, NCHN); (Found: C, 44.32; H, 4.90; N, 14.23. $C_{29}H_{38}N_8P_2F_{12}$ requires C, 44.17; H, 4.86; N, 14.21%).

Synthesis of bis{2,6-di(3-*n*-butylbenzimidazolin-2-ylidene)-4-diethylaminotriazine}disilver(I) bis(hexafluorophosphate) [(C^{tz}NC)$_2$Ag$_2$](PF$_6$)$_2$ 6·2PF$_6$. A mixture of **5**·2PF$_6$ (0.12 g, 0.15 mmol), Ag_2O (0.048 g, 21 mmol) and 3 Å molecular sieves in acetonitrile (15 mL) was stirred under nitrogen, in darkness, for 3 days. The mixture was then filtered through a plug of Celite and the filtrate was evaporated to dryness. The residue was triturated in ethyl acetate (15 mL) and the solid was collected and dried to afford a white powder (0.072 g, 64%). δ_H (400.1 MHz; CD_3CN) 0.34 (12 H, t, *J* 8 Hz, 4 × $CH_2CH_2CH_3$), 0.89 (8 H, m, 4 × $CH_2CH_2CH_3$), 1.12 (4 H, m, 4 × NCH_2CHHCH_2), 1.36 (4 H, m, 4 × NCH_2CHHCH_2), 1.46 (12 H, t, *J* 8 Hz, 4 × NCH_2CH_3), 3.98 (8 H, m, 4 × NCH_2CH_3), 4.20 (8 H, m, 4 × $NCH_2CH_2CH_2$), 7.54–7.65 (12 H, m, 12 × Ar*H*), 8.66 (4 H, d, *J* 8 Hz, 4 × Ar*H*); δ_C (100 MHz, CD_3CN) 13.2 ($CH_2CH_2CH_3$), 14.5 (NCH_2CH_3), 20.1 ($CH_2CH_2CH_3$), 32.6 ($NCH_2CH_2CH_2$), 44.4 (NCH_2CH_3), 51.1 ($NCH_2CH_2CH_2$), 113.5 (benzimidazolyl CH), 117.7 (benzimidazolyl CH), 126.7 (benzimidazolyl CH), 127.3 (benzimidazolyl CH), 132.9 (benzimidazolyl C), 135.4 (benzimidazolyl C), 164.4 (triazinyl C)

165.5 (triazinyl C) and 193.6 (two doublets, $^{1}J_{^{107}Ag,C}$ 187 Hz, $^{1}J_{^{109}Ag,C}$ 215 Hz, C–Ag); δ_H (600.1 MHz; d_6-DMSO) 0.26 (12 H, t, *J* 7 Hz, 4 × $CH_2CH_2CH_3$), 0.83 (8 H, m, 4 × $CH_2CH_2CH_3$), 0.99 (4 H, m, 4 × NCH_2CHH), 1.27 (4 H, m, 4 × NCH_2CHH), 1.48 (12 H, t, *J* 7 Hz, 4 × NCH_2CH_3), 3.98 (4 H, m, 4 × $NCHHCH_3$), 4.08 (4 H, m, 4 × $NCHHCH_3$), 4.33 (4 H, m, 4 × $NCHHCH_2$), 4.40 (4 H, m, 4 × $NCHHCH_2$), 7.62 (4 H, apparent t, splitting 8 Hz, 4 × Ar CH), 7.73 (4 H, apparent t, splitting 8 Hz, 4 × Ar CH), 7.89 (4 H, d, *J* 8, 4 × Ar CH) and 8.67 (4 H, d, *J* 8, 4 × Ar CH); δ_C (150.9 MHz; d_6-DMSO) 12.63 ($CH_2CH_2CH_3$), 12.64 (NCH_2CH_3), 18.8 ($CH_2CH_2CH_3$), 31.5 (NCH_2CH_2), 43.1 (NCH_2CH_3), 49.7 (NCH_2CH_2), 113.0 (benzimidazolyl CH), 116.2 (benzimidazolyl CH), 125.9 (benzimidazolyl CH), 126.2 (benzimidazolyl CH), 131.4 (d, $^{3}J_{Ag,C}$ 4 Hz, benzimidazolyl C), 134.2 (d, $^{3}J_{Ag,C}$ 6, benzimidazolyl C), 163.0 (triazinyl C1 and C3), 163.9 (triazinyl C5) and 192.4 (two doublets, $^{1}J_{^{107}Ag,C}$ 188, $^{1}J_{^{109}Ag,C}$ 217, C–Ag); Analytically pure colourless crystals were grown by the diffusion of vapours between neat ethyl acetate and a solution of the salt in acetonitrile. (Found: C, 46.60; H, 4.68; N, 14.63. $C_{58}H_{72}N_{16}Ag_2P_2F_6$ requires C, 46.47; H, 4.84; N, 14.97%). Colourless crystals of crystallographic quality were grown by the diffusion of vapours between neat diethyl ether and a solution of the salt in acetonitrile.

Synthesis of bis{2,6-di(3-*n*-butylbenzimidazolin-2-ylidene)-4-diethylaminotriazine}digold(I) bis(hexafluorophosphate) $[(C^{tz}NC)_2Au_2](PF_6)_2$ 7·2PF$_6$. A solution of **6**·2PF$_6$ (0.12 g, 0.08 mmol) and bromido(tetrahydrothiophene)gold(I) (0.04 g, 0.11 mmol) in acetonitrile (15 mL) was stirred at room temperature for 3 d in darkness, under nitrogen with 3 Å molecular sieves. The solution was filtered through Celite, which was then rinsed with acetonitrile (15 mL). The yellow filtrate was concentrated *in vacuo* affording a yellow powder (0.10 g, 74%). δ_H (400 MHz, CD_3CN) δ 0.34 (12 H, t, *J* 7.2 Hz, 4 × $CH_2CH_2CH_3$), 0.89 (8 H, m, 4 × $CH_2CH_2CH_3$), 1.17 (4 H, m 4 × NCH_2CHHCH_2), 1.38 (8 H, m, 4 × NCH_2CHHCH_2), 1.46 (12 H, t, *J* 7.0 Hz, 4 × NCH_2CH_3), 3.99 (m, 8H, 4 × NCH_2CH_3), 4.28 (4 H, m, 4 × $NCHHCH_2CH_2$), 4.41 (4 H, m, 4 × $NCHHCH_2CH_2$), 7.56–7.62 (12 H, m, 12 × ArH), 8.66 (4 H, d, *J* 8.4 Hz, 4 × ArH); δ_C (100 MHz, CD_3CN) δ 12.7 ($CH_2CH_2CH_3$), 12.9 (NCH_2CH_3), 19.7 ($CH_2CH_2CH_3$), 32.0 ($NCH_2CH_2CH_2$), 44.0 (NCH_2CH_3), 50.4 ($NCH_2CH_2CH_2$), 113.1 (benzimidazolyl CH), 117.0 (benzimidazolyl CH), 126.9 (benzimidazolyl CH), 127.1 (benzimidazolyl CH), 132.0 (benzimidazolyl C), 134.5 (benzimidazolyl C), 163.4 (triazinyl C) 165.2 (triazinyl C) and 191.7 (C–Au); (Found: C, 41.93; H, 4.23; N, 13.31. $C_{58}H_{72}N_{16}Au_2P_2F_6$·0.5$CH_3CN$ requires C, 41.74; H, 4.36; N, 13.61%). Colourless crystals of crystallographic quality were grown by the diffusion of vapours between neat diethyl ether and a solution of the salt in acetonitrile. During the crystallisation process a very small quantity of yellow crystals also deposited from solution. These crystals were identified as **8**·2PF$_6$ by single crystal X-ray studies.

Synthesis of chlorido{2,6-di(3-*n*-butylbenzimidazolin-2-ylidene)-4-diethylaminotriazine}-palladium(II) hexafluorophosphate $[(C^{tz}NC)PdCl]PF_6$ 9·PF$_6$. A mixture of palladium(II) chloride (0.14 g, 0.79 mmol) in acetonitrile (10 mL) was heated at reflux for 2 h. The solution was filtered and cooled. To the filtrate was added **6**·2PF$_6$ (0.23 g, 0.29 mmol) and the resulting mixture was stirred at room temperature for 3 d in darkness, under nitrogen with 3 Å molecular sieves. The solution was filtered through Celite, which was rinsed with acetonitrile (15 mL). The yellow filtrate was concentrated *in vacuo* to afford a yellow powder (0.43 g, 95%). Crystals suitable for X-ray diffraction studies were grown by diffusion of vapours between neat diethyl ether and an acetonitrile solution of the salt (0.16 g, 36%). δ_H (400 MHz, d_6-DMSO) 0.87 (6 H, t, *J* 7.4 Hz, 2 × CH_2CH_3), 1.32–1.45 (10 H, m, 2 × $CH_2CH_2CH_3$, 2 × NCH_2CH_3), 1.75 (4 H, m, 2 × $NCH_2CH_2CH_2$), 3.96 (4 H, q, *J* 7.2 Hz, 2 × NCH_2CH_3), 4.56 (4 H, t, *J* 7.6 Hz, 2 × $NCH_2CH_2CH_2$), 7.65 (2 H, apparent t, 7.2 Hz splitting, 2 × ArH), 7.74 (2 H, apparent t, 7.6 Hz splitting, 2 × ArH), 7.88 (2 H, d, *J* 8.4 Hz, 2 × ArH) and 8.30 (2 H, d, *J* 8.0 Hz, 2 × ArH); δ_C (100 MHz, d_6-DMSO) 12.6 (CH_3), 13.6 (CH_3), 19.2 (CH_2), 31.6 (CH_2), 44.5 (CH_2), 47.0 (CH_2), 113.7 (benzimidazolyl CH), 113.8 (benzimidazolyl CH), 127.1 (benzimidazolyl CH), 127.7 (benzimidazolyl CH), 128.8 (benzimidazolyl C), 133.4 (benzimidazolyl C), 160.0 (triazinyl C1 and C3), 162.8 (triazinyl C5) and 174.0 (C–Pd). (Found: C, 44.39; H, 4.57; N, 14.15. $C_{29}H_{36}N_8PdClPF_6$ requires C, 44.46; H, 4.63; N, 14.30%).

Synthesis of bis{2,6-di(3-*n*-butylbenzimidazolin-2-ylidene)-pyridine}digold(I) bis(tetraphenyl-borate) $[(C^{py}NC)_2Au_2](BPh_4)_2$ 11·2BPh$_4$. A solution of bromido(tetrahydrothiophene)gold(I) (0.035 g, 0.1 mmol) in acetonitrile (1 mL) was added to a solution of **10**·2BPh$_4$ (0.09 g, 0.05 mmol) in acetonitrile (20 mL). The mixture was stirred for 2 h and then filtered through Celite. The filtrate was concentrated *in vacuo.* The residue was dissolved in $CHCl_3$ and then diluted with hexanes to afford a colourless powder (0.070 g, 65%). δ_H (500 MHz, d_6-DMSO) δ 0.82 (12 H, t, *J* 7.4 Hz, 4 × CH_2CH_3), 1.30 (8 H, m, 4 × CH_2CH_3), 1.80 (8 H, m, 4 × NCH_2CH_2), 4.64 (8 H, m, 4 × NCH_2CH_2), 6.81 (8 H, m, *para* BPh_4), 6.95 (16 H, m, *meta* BPh_4), 7.21 (16 H, m, *ortho* BPh_4), 7.59 (apparent t, splitting 7.5 Hz, 4H, 4 × benzimidazolyl H), 7.65 (apparent t, splitting 7.3 Hz, 4H, 4 × benzimidazolyl H), 7.84 (d, *J* 8.2 Hz, 4H, 4 × benzimidazolyl H), 8.02 (d, *J* 8.2 Hz, 4H, 4 × benzimidazolyl H), 8.19 (d, *J* 7.9 Hz, 4H, 2 pyridyl H3), 8.44 (t, *J* 7.8 Hz, 2H, 2 × pyridyl H4); δ_C (125 MHz, d_6-DMSO) δ 13.4 (CH_2CH_3), 19.3 (CH_2CH_3), 31.7 (NCH_2CH_2), 48.5 (NCH_2CH_2), 112.5 (CH, benzimidazolyl), 112.9 (CH, benzimidazolyl), 121.2 (CH, pyridyl C3), 121.5 (CH_{para}, BPh_4), 125.3 (q, J_{C-B} 2.7 Hz, CH_{meta}, BPh_4), 125.4 (CH, benzimidazolyl), 125.6 (CH, benzimidazolyl), 131.2 (C, benzimidazolyl), 133.4 (C, benzimidazolyl), 135.5 (CH_{ortho}, BPh_4), 143.8 (CH, pyridyl C4), 148.5 (CH, pyridyl C2), 163.3 (q, J_{C-B} 49 Hz, C_{ipso}, BPh_4), 188.6 (C–Au); (Found: C, 64.96; H, 5.07; N, 7.42. $C_{102}H_{98}N_{10}Au_2B_2$ requires C, 65.18; H, 5.26; N, 7.45%). Colourless crystals of crystallographic quality were grown by the diffusion of vapours between a solution of hexanes and a solution of the salt in acetone.

X-ray structure determinations

Crystallographic data for the structures were collected at 100(2) K (180(2) K for 7·2PF$_6$) on an Oxford Diffraction Gemini or an Oxford Diffraction Xcalibur diffractometer fitted with Mo Kα

radiation. Following face-indexed absorption corrections and solution by direct methods, the structures were refined against F^2 with full-matrix least-squares using the program SHELXL-2014.[70] Anisotropic displacement parameters were employed for the non-hydrogen atoms. All hydrogen atoms were added at calculated positions and refined by use of a riding model with isotropic displacement parameters based on those of the parent atom.

Density functional theory calculations

Density functional theory (DFT) calculations were performed using the SIESTA code.[71] The electronic wave functions were expanded in a basis set of numerical atomic orbitals of double-zeta plus polarization (DZP) quality. The effective potentials due to the nucleus and core electrons were described using norm-conserving Troullier and Martins[72] pseudopotentials. The electron density was represented using an auxiliary basis consisting of a real-space mesh with a kinetic-energy cutoff of 300 Ry. Exchange–correlation was treated using the non-local van der Waals method vdW-DF2(rPW86).[73] Atomic coordinates and unit cells (where applicable) were fully optimized in all calculations to a force tolerance of 0.01 eV $Å^{-1}$. For the isolated complexes calculations were performed in a cubic box with sides of 30 Å to avoid interactions of molecules with their periodic images.

We have previously shown that this approach can accurately model geometries and energies of molecular crystals and molecules.[42,60] For molecular crystals, the interaction energy ($E_{\text{interaction}}$) was calculated using:

$$E_{\text{interaction}} = \frac{E_{\text{crystal+metal}}}{n} - E_{\text{metal}} - E_{\text{molecule}},$$

where $E_{\text{crystal+metal}}$ is the energy of the optimised molecular crystal containing the metal atom, E_{metal} is the energy of an isolated metal atom, E_{molecule} is the energy of an isolated molecule from the molecular crystal, and n is the number of molecules in the unit cell. As the counter-ions were not required for calculations of the isolated complexes, the cubic cell was charged accordingly. Basis set superposition errors (BSSE) were accounted for using the Counterpoise (CP) correction method.[74]

Acknowledgements

We thank Curtin University for a Research and Teaching Fellowship (to D. H. B.). Dr Max Massi is thanked for useful discussions. This work was supported by computational resources provided by the Australian Government through the Pawsey Centre under the National Computational Merit Allocation and the Pawsey Partner schemes.

References

1 F. E. Hahn and M. C. Jahnke, *Angew. Chem., Int. Ed.*, 2008, **47**, 3122–3172.
2 P. de Frémont, N. Marion and S. P. Nolan, *Coord. Chem. Rev.*, 2009, **253**, 862–892.
3 E. A. B. Kantchev, C. J. O'Brien and M. G. Organ, *Angew. Chem., Int. Ed.*, 2007, **46**, 2768–2813.
4 S. Díez-González, N. Marion and S. P. Nolan, *Chem. Rev.*, 2009, **109**, 3612–3676.
5 V. Dragutan, I. Dragutan, L. Delaude and A. Demonceau, *Coord. Chem. Rev.*, 2007, **251**, 765–794.
6 E. Colacino, J. Martinez and F. Lamaty, *Coord. Chem. Rev.*, 2007, **251**, 726–764.
7 N. Marion and S. P. Nolan, *Chem. Soc. Rev.*, 2008, **37**, 1776–1782.
8 C. Samajłowicz, M. Bieniek and K. Grela, *Chem. Rev.*, 2009, **109**, 3708–3742.
9 I. J. B. Lin and C. S. Vasam, *Coord. Chem. Rev.*, 2007, **251**, 642–670.
10 J. C. Garrison and W. J. Youngs, *Chem. Rev.*, 2005, **105**, 3978–4008.
11 K. M. Hindi, M. J. Panzner, C. A. Tessier, C. L. Cannon and W. J. Youngs, *Chem. Rev.*, 2009, **109**, 3859–3884.
12 M.-L. Teyssot, A.-S. Jarrousse, M. Manin, A. Chevry, S. Roche, F. Norre, C. Beaudoin, L. Morel, D. Boyer, R. Mahiou and A. Gautier, *Dalton Trans.*, 2009, 6894–6902.
13 L. Oehninger, R. Rubbiani and I. Ott, *Dalton Trans.*, 2013, **42**, 3269–3284.
14 P. V. Simpson, C. Schmidt, I. Ott, H. Bruhn and U. Schatzschneider, *Eur. J. Inorg. Chem.*, 2013, **2013**, 5547–5554.
15 T. Bernardi, S. Badel, P. Mayer, J. Groelly, P. de Frémont, B. Jacques, P. Braunstein, M.-L. Teyssot, C. Gaulier, F. Cisnetti, A. Gautier and S. Roland, *ChemMedChem*, 2014, **9**, 1140–1144.
16 F. E. Hahn, M. C. Jahnke, V. Gomez-Benitez, D. Morales-Morales and T. Pape, *Organometallics*, 2005, **24**, 6458–6463.
17 D. Pugh and A. A. Danopoulos, *Coord. Chem. Rev.*, 2007, **251**, 610–641.
18 M. Poyatos, J. A. Mata and E. Peris, *Chem. Rev.*, 2009, **109**, 3677–3707.
19 E. Peris and R. H. Crabtree, *Coord. Chem. Rev.*, 2004, **248**, 2239–2246.
20 D. Pugh, A. Boyle and A. A. Danopoulos, *Dalton Trans.*, 2008, 1087–1094.
21 K. Inamoto, J.-I. Kuroda, E. Kwon, K. Hiroya and T. Doi, *J. Organomet. Chem.*, 2009, **694**, 389–396.
22 F. Jean-Baptiste dit Dominique, H. Gornitzka, A. Sournia-Saquet and C. Hemmert, *Dalton Trans.*, 2009, 340–352.
23 T. Tu, J. Malineni and K. H. Dötz, *Adv. Synth. Catal.*, 2008, **350**, 1791–1795.
24 T. Tu, X. Bao, W. Assenmacher, H. Peterlik, J. Daniels and K. H. Dötz, *Chem. – Eur. J.*, 2009, **15**, 1853–1861.
25 D. H. Brown, G. L. Nealon, P. V. Simpson, B. W. Skelton and Z. Wang, *Organometallics*, 2009, **28**, 1965–1968.
26 D. H. Brown and B. W. Skelton, *Dalton Trans.*, 2011, **40**, 8849–8858.
27 K. D. M. MaGee, G. Travers, B. W. Skelton, M. Massi, A. D. Payne and D. H. Brown, *Aust. J. Chem.*, 2012, **65**, 823–833.

28 A. Poethig and T. Strassner, *Organometallics*, 2011, **30**, 6674–6684.
29 A. Poethig and T. Strassner, *Organometallics*, 2012, **31**, 3431–3434.
30 J. C. C. Chen and I. J. B. Lin, *J. Chem. Soc., Dalton Trans.*, 2000, 839–840.
31 A. Caballero, E. Díez-Barra, F. A. Jalón, S. Merino, A. M. Rodríguez and J. Tejeda, *J. Organomet. Chem.*, 2001, **627**, 263–264.
32 W. Zuo and P. Braunstein, *Organometallics*, 2012, **31**, 2606–2615.
33 Y.-F. Han, G.-X. Jin, C. G. Daniliuc and F. E. Hahn, *Angew. Chem., Int. Ed.*, 2015, **54**, 4958–4962.
34 Y.-F. Han, G.-X. Jin and F. E. Hahn, *J. Am. Chem. Soc.*, 2013, **135**, 9263–9266.
35 A. Rit, T. Pape and F. E. Hahn, *Organometallics*, 2011, **30**, 6393–6401.
36 D. Tapu, D. A. Dixon and C. Roe, *Chem. Rev.*, 2009, **109**, 3385–3407.
37 H. M. J. Wang and I. J. B. Lin, *Organometallics*, 1998, **17**, 972–975.
38 A. Caballero, E. Díez-Barra, F. A. Jalón, S. Merino and J. Tajeda, *J. Organomet. Chem.*, 2001, **617–618**, 395–398.
39 K. A. Wheeler and B. M. Foxman, *Mol. Cryst. Liq. Cryst.*, 1992, **211**, 347–360.
40 X. Liu, R. Pattacini, P. Deglmann and P. Braunstein, *Organometallics*, 2011, **30**, 3302–3310.
41 A. Herbst, C. Bronner, P. Dechambenoit and O. S. Wenger, *Organometallics*, 2013, **32**, 1807–1814.
42 D. J. Carter and A. L. Rohl, *J. Chem. Theor. Comput.*, 2014, **10**, 3423–3437.
43 R. Sabatini, E. Küçükbenli, B. Kolb, T. Thonhauser and S. de Gironcoli, *J. Phys.: Condens. Matter*, 2012, **24**, 424209.
44 A. Otero-de-la-Roza, V. Luaña, E. R. T. Tiekink and J. Zukerman-Schpector, *J. Chem. Theor. Comput.*, 2014, **10**, 5010–5019.
45 S. Ehrlich, J. Moellmann and S. Grimme, *Acc. Chem. Res.*, 2013, **46**, 916–926.
46 K. Berland, Ø. Borck and P. Hyldgaard, *Comput. Phys. Commun.*, 2011, **182**, 1800–1804.
47 B. Civalleri, C. M. Zicovich-Wilson, L. Valenzano and P. Ugliengo, *CrystEngComm*, 2008, **10**, 405–410.
48 M. Del Ben, J. Hutter and J. VandeVondele, *J. Chem. Theor. Comput.*, 2012, **8**, 4177–4188.
49 S. Feng and T. Li, *J. Chem. Theor. Comput.*, 2006, **2**, 149–156.
50 K. D. Nanda and G. J. O. Beran, *J. Chem. Phys.*, 2012, **137**, 174106–174112.
51 M. A. Neumann and M.-A. Perrin, *J. Phys. Chem. B*, 2005, **109**, 15531–15541.
52 A. M. Reilly and A. Tkatchenko, *J. Chem. Phys.*, 2013, **139**, 024705–024713.
53 J. van de Streek and M. A. Neumann, *Acta Crystallogr., Sect. B: Struct. Sci.*, 2010, **66**, 544–558.
54 J. Antony, R. Sure and S. Grimme, *Chem. Commun.*, 2015, **51**, 1764–1774.
55 T. Bereau and O. A. von Lilienfeld, *J. Chem. Phys.*, 2014, **141**, 034101–034112.
56 L. Kronik and A. Tkatchenko, *Acc. Chem. Res.*, 2014, **47**, 3208–3216.
57 A. Otero-de-la-Roza and E. R. Johnson, *J. Chem. Theor. Comput.*, 2015, **11**, 4033–4040.
58 T. Risthaus and S. Grimme, *J. Chem. Theor. Comput.*, 2013, **9**, 1580–1591.
59 M. J. Turner, S. Grabowsky, D. Jayatilaka and M. A. Spackman, *J. Phys. Chem. Lett.*, 2014, **5**, 4249–4255.
60 D. J. Carter and A. L. Rohl, *J. Chem. Theor. Comput.*, 2012, **8**, 281–289.
61 M. Ogden, A. Rohl and J. Gale, *Chem. Commun.*, 2001, 1626–1627.
62 L. Kong, G. Román-Pérez, J. Soler and D. Langreth, *Phys. Rev. Lett.*, 2009, **103**, 096103.
63 A. M. Walker, B. Civalleri, B. Slater, C. Mellot-Draznieks, F. Corà, C. M. Zicovich-Wilson, G. Román-Pérez, J. M. Soler and J. D. Gale, *Angew. Chem., Int. Ed.*, 2010, **49**, 7501–7503.
64 F. Malberg, J. G. Brandenburg, W. Reckien, O. Hollóczki, S. Grimme and B. Kirchner, *Beilstein J. Org. Chem.*, 2014, **10**, 1299–1307.
65 H. Schmidbaur and A. Schier, *Angew. Chem., Int. Ed.*, 2015, **54**, 746–784.
66 S. Sculfort and P. Braunstein, *Chem. Soc. Rev.*, 2011, **40**, 2741–2760.
67 Q.-X. Liu, L.-N. Yin, X.-M. Wu, J.-C. Feng, J.-H. Guo and H.-B. Song, *Polyhedron*, 2008, **27**, 87–94.
68 J. T. Thurston, J. R. Dudley, D. W. Kaiser, I. Hechenbleikner, F. C. Schaefer and D. Holm-Hansen, *J. Am. Chem. Soc.*, 1951, **73**, 2981–2983.
69 R. Uson, A. Laguna and M. Laguna, *Inorg. Synth.*, 1989, **26**, 85–91.
70 G. M. Sheldrick, *Acta. Crystallogr., Sect. C*, 2015, **71**, 3–8.
71 J. Soler, E. Artacho, J. Gale, A. García, J. Junquera, P. Ordejón and D. Sánchez-Portal, *J. Phys.: Condens. Matter*, 2002, **14**, 2745.
72 N. Troullier and J. L. Martins, *Phys. Rev. B: Condens. Matter*, 1991, **43**, 8861–8869.
73 K. Lee, É. Murray, L. Kong, B. Lundqvist and D. Langreth, *Phys. Rev. B: Condens. Matter*, 2010, **82**, 081101.
74 F. B. van Duijneveldt, J. G. C. M. van Duijneveldt-van de Rijdt and J. H. van Lenthe, *Chem. Rev.*, 1994, **94**, 1873–1885.

